Alternative method to study the radial dispersion in liquid chromatography columns. Part I: Theory

Vanderheyden, Yoachim; Broeckhoven, Ken; Desmet, Gert

Published in:
Journal of Chromatography A

DOI:
10.1016/j.chroma.2020.460868

Publication date:
2020

Alternative Method to Study the Radial Dispersion in Liquid Chromatography Columns. Part I: Theory

Yoachim Vanderheyden, Ken Broeckhoven, Gert Desmet*

Vrije Universiteit Brussel, Department of Chemical Engineering, Pleinlaan 2, 1050 Brussels, Belgium

**Corresponding author: Pleinlaan 2, 1050 Brussels, Belgium.*

Phone: (+)32.(0)2.629.32.51. Fax: (+)32.(0)2.629.32.48. E-mail: gedesmet@vub.ac.be

Abstract

We report on an alternative experimental method to determine the transversal or radial dispersion coefficient (D_{rad}) in packed bed columns for liquid chromatography. The method uses a recently developed type of column end-fitting with an impermeable segmentation ring that splits the incoming flow in a central and peripheral part. Using this device and continuously sending a tracer-laden flow through the central inlet and a tracer-less flow through the peripheral inlet, a steady-state radial dispersion pattern is established which can be used to determine the degree of radial dispersion.

The present part of the study lays the theoretical foundation for the method and shows the parameter sensitivity of the different possible data analysis variants. In addition, computational fluid dynamics simulations have been to validate the established procedure (agreement between true and determined D_{rad}-value better than 0.4%) as well as to study the effect of the most important error sources: the presence of the annular flow segmentation ring and the almost inevitable occurrence of mismatches between the central and the peripheral in- and outlet flows. In the latter case, a combined read-out method can be proposed that nearly perfectly compensates for the flow mismatch error (remaining error on the D_{rad}-value smaller than 3%).

1. Introduction

Liquid chromatography is probably the chemical process whose performance is most sensitive to the micro- and macroscopic shape of the column packing. This sensitivity manifests itself as the axial dispersion or band broadening, which directly determines the separation efficiency of the column. An important contributor to this axial dispersion originates from the radial differences in axial velocity that inevitably arise because of the non-uniformity of the medium (so called eddy-dispersion). Fortunately, these biases in axial velocity are countered by the radial dispersion process, tending to alleviate these axial velocity differences [1]. According to Fick's law, the radial dispersion process is quantified by the radial dispersion coefficient (D_{rad}), which hence plays a crucial role in determining the eventual degree of eddy-dispersion. Somewhat surprisingly, the number of studies value on the measurement of D_{rad} in chromatography columns and its dependency on the flow rate, particle size, retention factor, etc is relatively scarce, and there is no generally accepted model that can be used to accurately predict D_{rad} under a given specific condition. This is in part due to the fact that these columns are operated in a range of very low Reynolds-numbers (typically $Re < 0.01$) and reduced velocities (typically $0 < \nu < 20$), which are seldom encountered in other packed bed processes, such that the data found in engineering literature are of little use. The reduced velocity ν, also commonly known as the Péclet-number (Pe), is defined as the ratio of the rate of transport by convection to that by diffusion [1-3]:

$$\nu = Pe = \frac{u \cdot d_p}{D_{mol}} \tag{1}$$

with u the linear velocity, d_p the particle size and D_{mol} the molecular diffusion coefficient.

The common thread in all literature correlation is that D_{rad} can be described by an expression of the following form:

$$\frac{D_{rad}}{D_{mol}} = \frac{D_{eff}}{D_{mol}} + f(v) \tag{2}$$

wherein D_{eff} is the effective diffusion coefficient (=effective average over diffusion outside and inside particles) as measured by a peak parking experiment. Note that diffusion in a packed bed column can be assumed to be isotropic, hence the effective diffusion rate measured in the axial direction should be the same as in the radial direction. The second term represents the departure from D_{eff} in the presence of an advective transport component. Throughout the years, many different expressions have been suggested for f [4-8], with the most commonly adopted form being a simple linear proportionality. The latter appears to be the correct relationship at high velocities, but in the range of velocities applicable to packed bed LC the relationship appears to be more complex [7-8]. For example, video recordings of the radial dispersion in micro-pillar array chips covering the range of showed that D_{rad} rather follows an s-shaped curve, with

D_{rad} leveling off to a constant value again at high ν ($\nu > 50$). A good overview of the correlations and experiments typically used in engineering is given in [5].

Another important shortcoming of the D_{rad}-values and correlations found in classical engineering studies in the context of chromatography is that they do not incorporate the effect of species retention, which can be expected to play an important role in the radial transport in chromatography columns. Due to the retention equilibrium, the analytes spend a large part of their time in the retained state, during which they undergo an enhanced transport (so-called surface diffusion). Transport through the particle is given by the product of the diffusion in or on the stationary phase layer (which in itself is slower than in the bulk of the mesopores) and the equilibrium constant K. Given the latter can be much larger than unity, the so-called surface diffusion [9] can be expected to be a major contributor to the over-all intra-particle diffusion rate, and hence also to D_{rad}.

Given the above, there is a clear need for good methods to accurately measure D_{rad} in chromatographic columns. Unfortunately, the number of such studies is rather limited. Most measurements of the radial dispersion in packed bed columns are based on the measurement of the radial variation of the tracer concentration when injecting an instantaneous or continuous source of tracer [5,10-17]. Shalliker et al. proposed a method to measure D_{rad} with an in-column injection of a small droplet volume of tracer inside a transparent glass column using a needle [18]. Through optical measurement of the dispersion of this droplet in time, one can deduce the axial and radial dispersion coefficients. This technique has proven that radial differences in packing quality affect both axial and radial dispersion rates. This technique is however limited in inlet pressure and particle size since the use of large pressures to pack small particles can break the glass column. Furthermore, the use of pulsed-field-gradient nuclear magnetic resonance has been used to determine dispersion in packed bed columns [19-21], but this technique is limited to low fluid velocities [5].

In the present contribution, a radial dispersion coefficient measurement method is discussed that uses the flow segmentation or parallel segmented flow technology introduced a few years ago by Shaliker and co-workers [22-25]. This technology allows to split the flow running through the column in a central and a peripheral fraction, using in- and outlet frits containing an impermeable annular ring and connected to a dedicated end fitting piece having one central and three peripheral ports. Originally, the parallel segmented flow technology was used to reduce the trans-column velocity gradient band broadening originating from radial differences in packing density (including the so-called side-wall effect) and/or from

radial temperature gradients caused by viscous heating. In the present study, the device is used to experimentally measure the radial dispersion coefficient.

2. Proposed method

2.1 General method and mathematical modelling

The proposed measurement principle is depicted in Fig. 1. Spiking the mobile phase flow entering the central inlet port with a tracer analyte, while continuously sending pure mobile phase through the peripheral inlets, will establish a steady-state, diverging dispersion plume whose width solely depends on the species migration velocity and the degree of radial dispersion. Subsequently measuring the steady-state tracer concentration at the central and/or the peripheral outlet ports can then be used to extract the value of the radial dispersion coefficient D_{rad}, because a high degree of radial dispersion can be expected to lead to a high C_{peri} (i.e., just below or equal to C_{cent}) while a low degree of radial dispersion will keep a high C_{cent} (close to its inlet concentration) and lead to a low C_{peri}.

The measured concentration differences at the outlet of the central and peripheral (represented in Fig. 1 as flow C and P respectively) can be related to the D_{rad}-value by solving the following mass balance over the entire column [5,26]:

$$\frac{\delta C}{\delta t} = -\frac{u}{1+k''}\frac{\delta C}{\delta x} + D_{ax}\frac{\delta^2 C}{\delta x^2} + \frac{1}{r}\frac{\delta}{\delta r}\left(D_{rad}\cdot r\cdot\frac{\delta C}{\delta r}\right) \quad (3)$$

with D_{ax} and D_{rad} the effective axial and radial dispersion coefficient wherein the mobile phase dispersion and the intra-particle diffusion are weighted by the time spent inside (fraction k''/(1+k'')) and outside the particles (fraction 1/(1+k'')). Further, u is the interstitial velocity and k'' the zone retention coefficient defined as the ratio of the time spent and outside the particles [26]. In the proposed D_{rad}-experiment, the continuous flow and dispersion resulting from the continuous infusion of tracer through the central inlet of the column (leading to the boundary conditions $C/C_0 = 1$ at $r \leq R_c$ and $C/C_0 = 0$ at $r > R_c$ at $x = 0$) can be expected to result in a steady-state tracer 'dispersion plume' as depicted in Fig. 1. An observer moving with a cross-sectional plane with velocity u/(1+k'') will observe this plume in his observational plane as a gradually expanding circular spot. Considering furthermore that the convective axial transport is much stronger than the dispersive axial transport (Bodenstein number [27] already >1000 after the first few mm of the column), we can neglect the axial dispersion term and the mass balance in Eq. (3) for a moving observer becomes:

$$\frac{\delta C}{\delta t} = \frac{1}{r}\frac{\delta}{\delta r}\left(D_{rad}\cdot r\cdot\frac{\delta C}{\delta r}\right) \quad (4)$$

The analytical solution of this equation for the specific geometry of the current problem can be derived from [28,29], where the problem of the transient radial diffusion (of heat) for the case of an instantaneous tracer pulse applied in a circular infinitely thin ring with radius r' injected at t = 0 is solved for the case of a no-flux condition at the outer radius R, leading to:

$$C(r,r',t)=\frac{1}{\pi R^2}\sum_{n=1}^{\infty} e^{-D_{rad}\alpha_n^2 t}\frac{J_0(r\alpha_n)J_0(r'\alpha_n)}{J_0^2(R\alpha_n)+J_1^2(R\alpha_n)} \quad (5)$$

where α_n are the positive roots of $J_0(R\alpha_n) = 0$, and J_0 and J_1 are the Bessel functions of the first and second order respectively. These Bessel functions can be calculated using the standard Matlab®-function *besselj*. The values of α_n are calculated using the *besselzero.m* routine, written by von Winckel and freely available on Mathworks [30].

Before proceeding, it is instructive to note the time and the dispersion coefficient are tightly linked, cf. the appearance of the product $D_{rad}\alpha_n^2 t$ in the exponent of Eqs. (5). Given that also α_n can be expected to scale inversely proportional with R (cf. the appearance of the product $R.\alpha_n$ in the argument of J_0 and J_1), it is straightforward to introduce a dimensionless time t':

$$t'=\frac{t_R \cdot D_{rad}}{R^2} \quad (6)$$

Subsequently, Eq. (5) can be extended to account for the fact that the injection is not limited to an infinitely thin ring but homogeneously covers a full circular region with radius R_c. This is implemented by integrating Eq. (5) over the radius r', ranging from 0 to R_c. Also using Eq. (6), this finally yields:

$$C(r,t)=2\pi\int_0^{R_c}[C(r,r',t)]r'dr' \quad (7)$$

$$=\frac{2}{R^2}\sum_{n=1}^{\infty} e^{-R^2\alpha_n^2 t'}\frac{J_0(r\alpha_n)}{J_0^2(R\alpha_n)+J_1^2(R\alpha_n)}\int_0^{R_c} J_0(r'\alpha_n)r'dr'$$

Fig. 2 shows the typical behavior of the radial concentration profiles described by Eq. (7) for different values of t' for the case of a circular injection region with relative radius $R_c/R = 0.5$. The concentration profiles were normalized using the initial injection concentration ($C' = C/C_0$).

Fig. 2 readily reveals two limiting cases, both represented in blue. If the radial dispersion coefficient or the residence time tend to infinity ($t' = +\infty$), the injected tracer analytes are dispersed evenly across the column radius, thus leading to a radially uniform concentration (cf. blue line for t' = 0.5 in Fig. 2). To obey the conservation of mass, the concentration under this totally dispersed condition should be equal to the ratio of the area of the injected pulse (πR_c^2) versus the total column area (πR^2), which is 0.25 in this specific case. Comparing with the other considered t'-values, it can be concluded that a fully dispersed

flat concentration profile will be prevailing for all times t' larger than 0.5. When t' = 0.5, the maximal difference in concentration (i.e., the difference in concentration at the center (r = 0) and the concentration at the outer surface (r = R)) is already smaller than 0.1%.

In the other limiting case (t' = 0), when the time and/or the radial dispersion coefficient tend to zero, the concentration profile displays a straight step-function shape as the concentration in the central part (r' < R_c/R) is still equal to the maximal value of 1, while the concentration of tracer is zero everywhere else (r' > R_c/R). The wiggles [31] that are present in the solution for this limiting case, especially at radii close to R_c, originate from the summation over the parameter (n) in Eqs. (5) and (7), which should ideally be executed for an infinite number. Due to limitations in processing power and time, the counter n is however only calculated up to a value of 100.

For the intermediate values of t', the concentration profile is gradually changing from a step-function to a constant value with increasing t', as represented by the different colored lines in Fig. 2. Knowing these radial concentration profiles as a function of t', the average concentration at the outlet of the column in the central (C_{cent}) and peripheral (C_{peri}) part can be calculated by integrating Eq. (7) over the central, resp. peripheral part of the column outlet cross-section:

$$C_{cent} = \frac{1}{\pi R_c^2} \int_0^{R_c} [C(r,t)]\, 2\pi\, r\, dr \tag{8}$$

$$= \frac{1}{\pi R_c^2} \int_0^{R_c} \left[\frac{2}{R^2} \sum_{n=1}^{\infty} e^{-R^2 \alpha_n^2 t'} \frac{J_0(r\alpha_n)}{J_0^2(R\alpha_n)+J_1^2(R\alpha_n)} \int_0^{R_c} J_0(r'\alpha_n) r' dr' \right] 2\pi\, x\, dx$$

$$C_{peri} = \frac{1}{\pi(R^2-R_c^2)} \int_{R_C}^{R} [C(r,t)]\, 2\pi\, r\, dr \tag{9}$$

$$= \frac{1}{\pi(R^2-R_c^2)} \int_{R_c}^{R} \left[\frac{2}{R^2} \sum_{n=1}^{\infty} e^{-R^2 \alpha_n^2 t'} \frac{J_0(r\alpha_n)}{J_0^2(R\alpha_n)+J_1^2(R\alpha_n)} \int_0^{R_c} J_0(r'\alpha_n) r' dr' \right] 2\pi\, x\, dx$$

Both concentrations play a key role in the proposed method since they are the ones that are experimentally accessible when connecting the central and/or peripheral part of the column outlet to a detector. The course of C_{cent} and C_{peri} as a function of the dimensionless t' as determined by Eqs. (8) and (9) is represented by the full lines shown in Fig. 3 for the case of R_c/R = 0.5 (Fig. 3a) and R_c/R = 0.75 (Fig. 3b), both representative for the conditions considered in the experimental part of the study (see part II).

Again, the two limiting cases for very low and very high values of t' can be readily distinguished. At very low values of t', corresponding to very short residence times or small values of D_{rad}, no significant radial

dispersion takes place in the column and the average central outlet concentration C_{cent} is still equal to the concentration at the central inlet of the column (i.e., $C_{cent} = C_0$), whereas the average peripheral outlet concentration C_{peri} is equal to zero. For very high values of t' on the other hand, radial dispersion is complete, leading to a completely uniform distribution of tracer along the column, with $C'_{cent} = C'_{peri} = 0.25$ for the $R_c/R = 0.5$-case and $C'_{cent} = C'_{peri} = 0.57$ for the $R_c/R = 0.75$-case. Note that in general this fully dispersed concentration at large t' is equal to $(R_c/R)^2$).

For intermediate t', the normalized concentration profiles gradually vary between the two limiting cases. The course of this variation can be used as a calibration curve to determine the value of t', as is represented by the blue arrows in Fig. 3a. Using Eq. (7) and the known residence time (t_R) and column radius R, the value for D_{rad} can then be directly calculated from the thus determined value of t'.

2.2 Parameter sensitivity analysis and alternative data analysis methods

The sensitivity of the read-out of t' depends on the steepness of the C' versus t'-curve. Both the C'_{cent}- and C'_{peri}-curves vary most strongly, i.e., are most sensitive in the range of t'-values between 10^{-3} and 0.3. Since the actual value of t' is determined by the column parameters (D_{rad}, F, k'', R) and can hence not be selected by the user, it is important to have the possibility to shift the range of maximal sensitivity to other values. To pursue this, we combined the C'_{cent}- and C'_{peri}-values into a number of combined parameters (see dashed curves added to Fig. 3) such as for example their sum ($C'_{cent}+C'_{peri}$), abbreviated as the C+P-method, or their difference ($C'_{cent}-C'_{peri}$), abbreviated as the C-P-method. Both the C+P and the C-P method show the same sensitivity range as the pure C_{cent}- and C_{peri}-methods (i.e., largest steepness for $10^{-3} < t' < 0.3$). However, the C-P method has the advantage that this parameter changes over a larger C'-range (from 1 to 0) than either of both C_{cent} and C_{peri} methods. Also interesting is the C/P-method (based on the ratio C_{cent} and C_{peri}) as this shifts the range of maximal sensitivity to a totally different range of t'-values, i.e., ranging between $5 \cdot 10^{-7}$ and $5 \cdot 10^{-3}$. A drawback of these combined methods of course is that they depend on two parameters, thus adding to their absolute and relative measurement error. The product of C_{cent} and C_{peri} is to be discarded as a potential read-out method because it does not always vary monotonically (cf. the C·P-curve in Fig. 3a).

Important to note is that the course of the curves in the C' versus t' calibration plot depends on the radius R_c of the injection zone. This can be seen by comparing Fig. 3a with Fig. 3b, showing the C' versus t' plot for the case of a different R_c ($R_c/R = 0.75$). The C_{cent}- and C_{peri}-method now converge to a different value in the large t'-limit, again given by the ratio of the injected over the total inlet area $(R_c/R)^2$, which in this case is equal to 0.57. As a consequence, the C_{peri}-method has an increased sensitivity for the

determination of t', as now the C_{peri}-calibration curve varies over a larger range, i.e., from 0 to 0.57 instead of from 0 to 0.25 as is the case when $R_c/R = 0.5$. On the other hand, the sensitivity of the C_{cent}-method is decreased since the range of the central relative concentration is now only changing between 1 and 0.57 instead of between 1 and 0.25. As a consequence, also the derived quantities (C+P, C·P, C/P) display a different shape and have slightly different sensitivities.

In a more quantitative approach, the sensitivity of a given D_{rad} read-out method can be expressed as the ratio of the variation in D_{rad} that is read-out from the calibration curve in response to a variation in the measured C'-value:

$$\frac{\Delta D_{rad}}{\Delta C'} \cong \frac{dD_{rad}}{dC'} \Rightarrow \frac{\Delta D_{rad}}{D_{rad}} \cong \frac{dD_{rad}}{dC'}\frac{\Delta C'}{D_{rad}} \tag{10}$$

Since D_{rad} is proportional to t' (see Eq. 6), this leads to:

$$\frac{\Delta D_{rad}}{D_{rad}} \cong \frac{dt'}{dC'}\frac{\Delta C'}{D_{rad}} \cong \frac{dt'}{dC'}\frac{1}{t'}\cdot\Delta C' \tag{11}$$

Eq. (11) shows a maximal sensitivity is obtained when the absolute value of the factor 1/t'·dt'/dC' becomes maximal. Fig. 4 shows the sensitivity curves for the two R_c/R-cases considered in Figs. 3a and 3b. As can be noted, the $R_c/R = 0.75$-geometry makes the C_{peri}-method slightly more sensitive compared to the $R_c/R = 0.5$-geometry, while the opposite occurs for the C_{cent}-method. In both cases, the read-out is maximally sensitive for t'-values around t' = 0.05. Reading out D_{rad} from the C-P-curve provides a higher sensitivity than any of the two basic curves, while the C+P-curve always leads to a lower sensitivity and is hence less useful. As already remarked before, the C/P-curve provides an opportunity to make sensitive measurements at much lower t'-values (region $t' = 10^{-5}$), i.e. at very high flow rates or very low radial dispersion rates.

3. Numerical methods

To investigate the deviations from the ideal situation considered in the previous section, a numerical simulation study was performed using the computational fluid dynamic (CFD) software package Ansys Fluent®. The Design Modeler and Meshing-module of this software package was used to draw and discretize the geometry of the column and the parallel segmented in- and outlet system. Subsequently this geometry was spatially discretized (=meshed) to calculate the velocity field and the species dispersion. The mesh cell size was chosen such that the velocity and mass profiles were independent of this size. It was found that $4.5\cdot10^5$ cells or nodes sufficed to produce a value for D_{rad} that was within a 0.3% accuracy of the case wherein the number of cells was quadrupled to $1.8\cdot10^6$.

Given the cylindrical symmetry of the column, the geometry was reduced to an axi-symmetrical problem calculated in cylindrical coordinates. Both the central and peripheral inlet boundaries were defined as a velocity inlet, whereas both outlets were defined as a pressure outlet. Two different column geometries (both with an radius of 2.3 mm) were considered: one with and one without the presence of a distributor ring (situated between 1.18 mm < r < 1.80 mm). The packed bed inside the column was modeled as a continuous porous region having an average viscous resistance (equal to the inverse of the column bed permeability) equal to 10^{14} m^{-2}, which can be considered as a representative value for a 3 µm particle bed. The material properties (e.g., viscosity, density, etc.) of the fluid and the tracer compound in the system were chosen equal to those of pure water. The radial mass diffusion coefficient of this tracer in the porous zone filled with fluid can be chosen in Fluent® by using a user defined diffusion function. This was used to vary D_{rad} over the range between $6 \cdot 10^{-10}$ m^2/s and $2 \cdot 10^{-9}$ m^2/s.

The CFD Fluent® software was used to first calculate the steady-state velocity field by solving the Navier-Stokes equations. Subsequently, the steady-state tracer species distribution was calculated solving the general advection-diffusion mass balance. The velocity and mass profiles were calculated using the segregated pressure-based steady state solver with a least squares cell based gradient evaluation and a second order upwind interpolation scheme for the momentum equations.

4. Numerical validation and influence of system parameters

4.1. Effect of the presence of the flow segmentation ring

As elaborated in the previous sections, the ratio of the injected over the total column radius R_c/R plays a key role in the analysis and the sensitivity of the experiment. In practice, the flow is split in two portions by the presence of the flow distributor ring which has a significant thickness. This leads to a disturbance of the flow, such that the position of the R_c-radius delimiting the injected tracer region is only established after a certain (short) distance downstream of the inlet distributor (see Fig. 6 further on for more detail). The streamlines running through the bed zone can be divided in two separate groups, resp. originating from the central (tracer) flow and the peripheral flow, and separated by an imaginary line, further referred to as the split line (Fig. 5). As this line also delimits the region accessible to the tracer in the absence of any dispersion, the radial position of this split line corresponds to the R_c-value appearing in Eqs. (7-9).

The radial position of the split line can be manipulated by changing the ratio of the central and peripheral flow rates because the conservation of mass dictates that the split line radius R_c is determined by the ratio of the central ($F_{c,in}$) to the total ($F_{c,in}+F_{p,in}$) flow rate:

$$\frac{R_c^2}{R^2} = \frac{F_{c,in}}{F_{c,in}+F_{p,in}} = \frac{F_{c,in}}{F_{tot,in}} \quad (12)$$

Eq. (12) shows that, for example, an increase in the relative central flow rate ($F_{c,in}/F_{tot,in}$) results in an increased split radius R_c, since the increased central inlet flow ($F_{c,in}$) forces the streamlines in the column to expand more towards the outer peripheral region.

In below part, the CFD software is used to validate the expressions given in Eqs. (8-9) without and with the potential disturbance of the distributor ring. In the former case, the flow going through the frit is divided in a central and peripheral fraction by assuming an infinitely thin distributor ring, capable of splitting the flow, but without disturbing the velocity profile. Figs. 6a-b compare the dispersion plume obtained in both cases. Both concentration contour plots strongly resemble the expected pattern represented schematically in Fig. 1. The tracer concentration is represented in color, with 100% tracer being blue and 0% tracer being red. Zooming in on the column inlet (Fig. 6c-d), some small differences between both cases becomes apparent, the most obvious one being the upward shift of the green colored zone reduced (C' = 0.5), representing the plane where the central and peripheral zone meet. This is further emphasized in Fig. 6 with the dashed horizontal line at radius r = R_c (split line radius, definition: see Fig. 5). The difference in position of the r = R_c-line between both cases owes to the fact that these cases were simulated by imposing a uniform velocity over the column inlet cross-section. Because of this uniform velocity, the flow rate going through the central and the peripheral part of the inlet cross-section is different with or without the presence of the thick distributor ring (because of the difference in cross-sectional area ratio between both cases). In the latter case, a relatively higher fraction of the flow goes through the center compared to the infinitely thin distributor ring-case because the ratio of the central to the peripheral cross-sectional inlet area is larger in the thick ring-case. This pushes the split line upward. It could be verified that the observed position of the split line was within the simulation accuracy (<0.1%) equal to that predicted by Eq. (12) when using the (exactly known) central and peripheral inlet flow rates. This holds for both the infinitely thin and the real distributor ring case.

An exact knowledge of the position R_c at which both central and peripheral flow paths are separated or split from each other is very important because the value of R_c strongly affects the shape of the C' versus t'-curves (see Fig. 3 for examples). When the numerical simulation was converged, the value of the tracer concentration at the outlet of column was averaged over the central and peripheral outlets and used to read out the corresponding value of t' from the C_{peri}- and C_{cent}-calibration lines. Since also the linear velocity u is exactly known in these CFD-simulations, the residence time t_R needed in Eq. (6) could be calculated as t_R = u/L, allowing to finally calculate the radial dispersion coefficient D_{rad} from the read-out

t'-value. In the CFD simulations, also the true D_{rad}-value is exactly known because this is numerically imposed via one the CFD subroutines. For the infinitely thin distributor ring case, we could establish that the error made via the D_{rad} read-out method elaborated in the discussion of Fig. 3 is below 0.4% for all proposed read-out methods (cf. the C_{cent}-, C_{peri}-, C/P-, C+P- and C-P- methods), thus validating the analytical expressions and methods proposed there.

Important to note next is the radial displacement of the streamlines occurring in the finite ring thickness case (Fig. 6f). The fact that the streamlines no longer run perfectly parallel is a potential problem that needed a detailed investigation, for it implies the presence of the ring induces an extra radial convective flow which can potentially offset the measured D_{rad}-value. Fortunately, the length over which the velocity disturbances occur is very short compared to the overall length of the column. A detailed inspection of Fig. 6f shows the streamlines become fully flat again after some 1.5-2 mm downstream of the end of the distributor ring. In a 75 mm long column, this only corresponds to 2-2.5% of the total length. This probably explains why the maximal error made on the read-out D_{rad}-value was found to be only marginally higher (0.5% vs 0.4%) than without the distributor ring present.

4.2. Impact of a mismatch between $F_{c,in}$ and $F_{c,out}$

As already indicated, a correct measurement of D_{rad} requires the streamlines in the column to run substantially parallel. This condition can only be achieved if the flow rate leaving the column through the central outlet is identical to the flow rate entering the column through the central inlet ($F_{c,in} = F_{c,out}$). This automatically also implies that, under conditions of an unchanging density, the same condition should hold for the peripheral flow ($F_{p,in} = F_{p,out}$). According to Eq. (12), this condition implies the value of R_c is independent of the axial position and is hence also the same at the column in- and outlet.

In case of a mismatch between the in- and outgoing flow rate, the streamlines can be expected to either converge or diverge along the column axis because a mismatch between the in- and outgoing flow in the central column part will inevitably induce a net advective radial transport component. The latter is to be prevented for it will disturb the measured radial transport and lead to observed D_{rad}-values deviating from the true radial dispersion rate prevailing in the absence of flow rate mismatch. In the latter case, the net flux of tracer across the split line can be written as:

$$\text{Flux} = \Omega \cdot D_{rad,true} \frac{<\Delta C>}{R} + <C_c> \cdot \Delta F_c = \Omega \cdot D_{rad,obs} \frac{<\Delta C>}{R} \qquad (13)$$

wherein the radial dispersion through the mantle surface of the split line area ($\Omega = \pi R_c^2$) depends on the difference in radial tracer concentration $<\Delta C>$ and wherein the advective transport through this surface is

the product of the difference in central flow rate ($\Delta F_c = F_{c,in}-F_{c,out}$) and the average tracer concentration $<C_c>$ in the central zone. Whereas Eq. (13) readily shows the observed $D_{rad,obs}$ will differ from $D_{rad,true}$ in the presence of a net advective transport going from the central to the peripheral region or vice-versa, it is of little practical use because there exist no simple expressions for $<\Delta C>$ and $<C_c>$.

Unfortunately, mismatches in flow between the inlet and outlet are difficult to avoid, because this requires that the average flow resistances of the three peripheral connection tubing capillaries needs to be exactly the same as the flow resistance of the central connection tubing, on both the in- an outlet side. In part II, it is shown this is very difficult to realize in practice, especially when considering the connection tubing flow paths at the outlet need to pass through a detector. Other deviations result from errors on the read-out of the mass flow meters, the inaccuracy of the pumped flow rate and thermal fluctuations.

In below part, we show the results of a series of CFD simulations conducted to investigate the effect of flow rate mismatches by imposing an exactly known flow rate error ($\Delta F_c = F_{c,in}-F_{c,out}$) and subsequently comparing the measured with the true D_{rad}-value (which is exactly known as it is imposed numerically). The mismatch was induced by introducing an additional pressure drop in either the central or peripheral outlet of the column to change the ratio of the relative central flow rate between the inlet and outlet of the column. The simulations show that an increase in pressure resistance at the peripheral outlet results in a higher relative central outlet flow rate, in turn resulting in a streamline pattern converging towards the central column outlet. Obviously, this affects the tracer concentration measured at the peripheral and central outlets. It was found that when $F_{c,out} > F_{c,in}$ (i.e., central converging streamlines), an increased amount of peripheral streamlines (carrying lower concentrations of tracer) is going through the central outlet, thus decreasing the central outlet tracer concentration. The flow at the peripheral outlet will consequently only consist of the most outward streamlines (carrying the lowest concentration of tracer), such that also the peripheral outlet concentration will be decreased. Similarly, when $F_{c,out} < F_{c,in}$ the central streamlines will gradually diverge along the column axis and an increased amount of central streamlines (carrying high concentrations of tracer) will leave the column through the peripheral column outlet. Because the outer streamlines of the central region carry a lower concentration of tracer compared to the most central streamlines (i.e., due to radial dispersion), the loss of the lowest concentrations leads to a situation where also the concentration in the central column outlet increases.

Although the above observations (concentration values in central and peripheral outlet either both decrease or both increase upon a change in relative central flow rate at the column outlet) may appear unexpected, they do not violate the law of conservation of mass. Considering for example the case of

central converging streamlines, the decrease in tracer concentration in the central outlet is more than compensated by the increase in flow rate, resulting in a larger mass flux of tracer through the central outlet. Together with a lower peripheral mass flux (since both concentration of tracer and flow rate is decreased), the sum of both mass fluxes is still equal to the case without a flow ratio disturbance.

The impact of the change in average central and peripheral concentrations on the extracted D_{rad}-values is best visualized when interpreting the example C' versus t'-plot shown in Fig. 7, representing the same R_c/R = 0.5-case as considered in Fig. 3.

Considering first the case of converging central streamlines (flow resistance in central outlet smaller than in peripheral outlet). In this case, the lower concentration in the central outlet (C_{cent}) results in the read-out of a higher t', thus overestimating D_{rad} (see green arrows added to Fig. 7). The lower C_{peri} on the other hand results in the read-out of a lower t' and hence underestimates the value of D_{rad}. I.e., depending on the selected read-out method, the flow rate mismatch will either lead to an over- or an underestimation. A similar situation arises for the case with an increased central outlet pressure resistance (diverging central streamlines). This results in higher concentrations of tracer in both central and peripheral outlet. As shown by the green arrows in Fig. 7, this leads to an underestimation of D_{rad} when using the C_{cent}-method and to an overestimation of D_{rad} when using the C_{peri}-method.

The above analysis has been repeated for a series of differently imposed flow rate mismatches, always using a total flow rates and a $D_{rad,true}$-value corresponding to t' = $1.1 \cdot 10^{-2}$. The final result is shown in Figure 8, plotting the ratio of the observed versus the true D_{rad} ($D_{rad,obs}/D_{rad,true}$) as a function of the imposed error on the central outlet-to-inlet ratio for the different read-out methods represented in Fig. 3. The right hand side of this curve (relative central outlet flow rate higher than the relative central inlet flow rate, $F_{central,outlet} > F_{central,inlet}$) represents the case of central converging streamlines, the left hand side represents the case of central diverging streamlines ($F_{central,outlet} < F_{central,inlet}$). The C' versus t' plots needed to calculate D_{rad} were always established using Eqs. (8-9) using the proper value of the split radius R_c as read-out at the inlet of the column.

As can be noted, the overestimation of the C_{cent}-method and the underestimation of the C_{peri}-method (in the case of central converging streamlines) varies quasi linearly with the error on the central outlet-to-inlet flow ratio over the entire investigated range of relative flow mismatch rates. This is emphasized by the straight dotted lines added to guide the eye, and representing the linear best fit passing through the x=0-point at the $D_{rad,obs}/D_{rad,true}$=1-point. As the $D_{rad,obs}/D_{rad,true}$-values have been obtained via CFD-

simulations where $D_{rad,true}$ and all flow rates are exactly known, these lines can now be used to correct the experimentally determined D_{rad}-values for the experimentally observed flow mismatch, multiplying the observed D_{rad}-value with the $D_{rad,obs}/D_{rad,true}$-ratio read-out from Fig. 8 for the corresponding relative flow mismatch.

The quality of all D_{rad} read-out techniques can now be compared, with the C-P method resulting in the smallest error (i.e., the cyan line lies closest to the hypothetical horizontal black line, representing the ideal case where no correction would be needed). Even more interesting to see is that the overestimation (or underestimation) factor of the C_{cent} method is almost equal to the underestimation (or overestimation) factor of the C_{peri}-method. This finding led us to the introduction of yet another read-out method, abbreviated by $CP_{average}$. This method simply calculates the average of the D_{rad} values read-out from the C_{cent}- and C_{peri}-calibration curves. The result is represented by the gray crosses in Fig. 8. These all lie very close to the perfect horizontal $D_{rad,obs}/D_{rad,true}$=1-line, implying the $CP_{average}$-method allows to closely approach the true D_{rad}, even when $F_{c,in} \neq F_{c,out}$, i.e., even when the streamlines do not run perfectly parallel with the column axis. Considering the sensitivity study in Fig. 4, where the change in sensitivity of the C_{cent}-and the C_{peri}-method resulting from a change in R_c/R-value behave as “communicating vessels” (sensitivity gain of the one is nearly exactly matched by a concomitant loss of the other), it can also be inferred the sensitivity of the $CP_{average}$-method will be roughly the same over the entire range of possible relative central flow rates (i.e., for all possible imposed R_c/R-value). This constitutes another important advantage.

As discussed in Section 2, the sensitivity of the employed D_{rad} read-out method depends on the value of t', and this value is to a large extent imposed by the system and cannot be chosen by the experimentalist. Additional CFD-calculations have therefore been made for two other t'-values: one larger and one smaller (resp. $t' = 2 \cdot 10^{-2}$ and $t' = 5 \cdot 10^{-3}$). The analysis of these measurements resulted plots of the $D_{rad,obs}/D_{rad,true}$-value (results not shown) similar to Fig. 8. It was found that the slopes of the $D_{rad,obs}/D_{rad,true}$-error lines increased with about 5% for the lower value of t' ($t' = 5 \cdot 10^{-3}$), and decreased by 2-3% for the higher value of t' ($t' = 2 \cdot 10^{-2}$). (compared to the results shown in Fig. 8 where a value of $t' = 1.1 \cdot 10^{-2}$ is used). This holds for both the C_{cent} and C_{peri}-method. As a consequence, the impact of the difference in t' on the outcome of the $CP_{average}$-method remained very small, confirming this method as the most accurate D_{rad} read-out method.

Obviously, the above only holds for the range of flow rate mismatches considered in Fig. 8 and one should be very cautious about making a linear extrapolation outside the investigated range.

5. Conclusions

The end fitting pieces enabling to split the flow in a central cylindrical flow and peripheral annular sheath flow introduced a few years ago can be used to devise a method to determine the radial dispersion coefficient in liquid chromatographic columns. Using the device, a continuous injection of tracer through the central inlet of the column establishes a steady-state concentration profile with radially diverging tracer concentration (see Fig. 1). Once steady-state is reached, the tracer concentration measured in the central and peripheral outlet can be used to calculate D_{rad}. The solution of the dispersion problem for an observer moving with the same speed as the tracer is giving by Eq. (9) and has led to the introduction of calibration curves (cf. the C' versus t' curves shown in Fig. 3), linking the measured normalized tracer concentrations to a dimensionless time $t' = t_R \cdot D_{rad}/R^2$, wherein D_{rad} is then left as the only unknown.

Using computational fluid dynamic (CFD) software, the proposed experimental approach (including the real-world effect of the finite segmentation ring thickness and the quasi inevitable occurrence of flow rate mismatches) was numerically simulated and the agreement with the analytical models was validated. It has been found that the presence of the flow distributor ring does not significantly disturb the measured value of D_{rad} and the analytical model can be accurately used providing the split line (=the imaginary line separating the streamlines belonging respectively to the central and the peripheral flows running through the column) runs perfectly parallel to the column axis, i.e., provided $F_{c,in} = F_{c,out}$ (which also implies that $F_{c,in} = F_{c,out}$). In case of a flow mismatch the C' versus t'- calibration curves can be best read-out via the $CP_{average}$-method. This method combines the information of the central and peripheral outlet concentrations in a way that nearly perfectly compensates for the flow mismatch error. With this approach, the remaining error on the D_{rad}-value is smaller than 3% over the entire range of investigated mismatches ($F_{C,out}$ max. 6% larger or smaller than $F_{C,in}$).

As a final comment, it should be noted the same approach could also be applied to measure the radial heat transfer coefficient (λ_{rad}), injecting heat instead of a tracer species, and measuring temperatures rather than concentrations. Knowing the value of λ_{rad} in chromatographic columns is also a timely problem because of the clear trend towards the use of ultra-high inlet pressures and the concomitant problem of radial temperature gradients that tend to affect column efficiency [32].

Figure Captions

Figure 1: (a) *Schematic representation of the proposed D_{rad}-measurement principle consisting of centrally injecting a tracer flow (blue) and measuring the tracer concentration in both the central (C) and peripheral flow (P).* **(b)** *Cross-sectional view of the specially designed end-fitting pieces needed to conduct the experiment. R_c is the radius of the central flow zone.*

Figure 2: *Normalized concentration profiles calculated using Eq. (7) as a function of the relative radius for seven values of the dimensionless time t' (t' = $D_{rad} \cdot t_R/R^2$) for the case of central tracer injection with relative radius $R_c/R = 0.5$.*

Figure 3: *Relative tracer concentration C' in the central (C_{cent}) and peripheral (C_{peri}) outlet as a function of $t' = t_R \cdot D_{rad}/R^2$ for the case of a relative central injection radius* ***(a)*** *$R_c/R = 0.5$ and* ***(b)*** *$R_c/R = 0.75$. Additional combinations of both C_{cent} and C_{peri} are represented in dashed lines: C_{cent}-C_{peri} (C-P), $C_{cent} \cdot C_{peri}$ (C·P), C_{cent}+C_{peri} (C+P) and C_{cent}/C_{peri} (C/P). The latter parameter is normalized with its maximal value at t' = 0 (814 for $R_c/R = 0.5$* ***(a)****, and 295 for $R_c/R = 0.75$* ***(b)****) to fit on the same normalized scale of the other parameters. The blue arrows added to* ***(a)*** *show the procedure to read out the value of t' at a given C_{cent}.*

Figure 4: *Sensitivity curves dC'/dt'·t' versus t', displaying the sensitivity of the D_{rad} read-out (using the C' versus t' plots shown in Figure 3) for the C_{cent}- and C_{peri}-method (full lines) as well as for the different composite measures considered in Fig. 3 (dashed lines). Relative central injection radius $R_c/R = 0.5$* ***(a)*** *and $R_c/R = 0.75$* ***(b)****.*

Figure 5: *Schematic representation of the flow pattern in a segmented parallel flow column with in- and outlet frits pierced by an impermeable ring (1). The streamlines (full lines) corresponding to the central (F_c) and peripheral (F_p) flow are separated by an imaginary split line (dashed line) positioned at a radius R_c. Width over length dimensions not to scale.*

Figure 6: *Visualization of the contour plots of the spatial tracer distribution (radial position versus axial coordinate x)* **(a-d)** *and the flow streamlines* **(e-f)** *calculated by the computational fluid dynamics software Ansys Fluent® (see section 3). Both a column with* **(b/d/f)** *and without* **(a/c/e)** *a distributor ring is presented.* **(c-f)** *show a zoom-in of the column inlet, the region in which differences in flow streamlines and split radius is most pronounced. Tracer concentrations range from 0% (red) to 100% (blue). The x-axis (i.e., the column length) in figures* **(a-b)** *is compressed with a factor of 3.3 in order to aid visualization. The split line (at relative split radius of $R_c/R = 0.5$) is indicated by the dashed line (relative central flow rate ($F_{c,in}/F_{tot,in}$) equals 0.25).*

Figure 7: *C' versus t' plot for the case of a relative central flow rate of 25% (corresponding to* $R_c/R = 0.5$ *with $R_c = 1.19$ mm and R = 2.39 mm). The effect of central converging (red arrows) and central diverging (green arrows) streamlines is shown on the D_{rad} read-out of the C_{cent} and C_{peri} method.*

Figure 8: *Plot of $D_{rad,obs}/D_{rad,true}$ versus the imposed error on the central outlet-to-inlet ratio for the case of $t' = 1.1 \cdot 10^{-2}$.Positive x-values represent the case of central converging streamlines, negative representing the region with diverging streamlines. Colour code for the data points relates to the different methods that can be used to read-out the C' versus t' plots: C_{cent} (♦), C_{peri}(■), C-P (●), C+P (x), C/P (▲). The gray crosses represent the new*

method introduced in the discussion of this figure: $CP_{average}$ (+). The horizontal black line represents the hypothetical perfect case where no correction is needed. Linear fits (dashed lines) are added to guide the eye.

References

[1] L Knox J.H., Band dispersion in chromatography–a new view of A-term dispersion, J. Chromatogr. A, 831 (1999) 3-15.
[2] G. Guiochon, A. Felinger, A. Katti, D. Shizazi, Fundamentals of preparative and nonlinear chromatography, 2nd ed., Academic Press, Boston, MA, 2006.
[3] U.D. Neue, HPLC Columns, Theory, Technology and Practice, Wiley VCH, New York 1997.
[4] T. Baron, Generalized graphical method for the design of fixed bed catalytic reactors, Chem Eng Prog, 48 (1952), 118-124.
[5] J.M.P.Q. Delgado, Heat Mass Transfer, 42 (2006), 279-310.
[6] D.J. Gunn, C. Pryce C, Theory of axial and radial dispersion in packed beds, Trans IChemE 47 (1969).
[7] S. De Bruyne, W. De Malsche, S. Deridder, H. Gardeniers, G. Desmet, In situ measurement of the transversal dispersion in ordered and disordered two-dimensional pillar beds for liquid chromatography, Anal. Chem., 86 (2014), 2947-2954.
[8] P.C. Saffman, Dispersion due to molecular diffusion and macroscopic mixing in flow through a network of capillaries, J Fluid Mech 7(1960) 194–207.
[9] K. Miyabe, G. Guiochon, Surface diffusion in reversed-phase liquid chromatography, J. Chromatogr. A 1217 (2010) 1713–1734.
[10] J.H. Knox, G.R. Laird, P.A. Raven, Interaction of radial and axial dispersion in liquid chromatography in relation to the infinite diameter effect, J. Chromatogr. 122 (1976) 129-145.
[11] G.A. Robbins, Methods for determining transverse dispersion coefficients of porous media in laboratory column experiments, Water Resour. Res. 25 (1989)1249–1258.
[12] R.R. Rumer, Longitudinal dispersion in steady and unsteady flow, J Hydr Div Proc Am Soc Civ Eng 88 (1962) 147–172.
[13] V.P. Dorweiler,R.W. Fahien, Mass transfer at low flow rates in a packed column, AIChE J 5 (1959)139–144
[14] R.W. Fahien, J.M. Smith, Mass transfer in packed beds, AIChE J 1 (1955) 28–37
[15] D.R.F. Harleman, R. Rumer R, Longitudinal and lateral dispersion in an isotropic porous medium, J Fluid Mech 16 (1963) 1-12.
[16] J.W. Hiby, P. Schummer P, Zur Messung der transversalen effektiven Diffusion in durchströmten Füllkörpersäulen, Chem Eng Sci 13 (1960) 69–74.
[17] J.H. Knox, J.F. Parcher, Effect of the column to particle diameter ratio on the dispersion of unsorbed solutes in chromatography. Anal. Chem. 41 (1969) 1599-1606
[18] R.A. Shalliker, B. Scott Broyles, G. Guiochon, Axial and radial diffusion coefficients in a liquid chromatography column and bed heterogeneity, J. Chromatogr. A 994 (2003) 1-12.
[19] U. Tallarek, K. Albert, E. Bayer, G . Guiochon, Measurement of transverse and axial apparent dispersion coefficients in packed beds, AIChE Journal 42 (1996), 3041-3054.
[20] E. Baumeister, U. Klose, K. Albert, E. Bayer, Determination of the apparent transverse and axial dispersion coefficients in a chromatographic column by pulsed field gradient nuclear magnetic resonance, J Chromatogr A 694 (1995) 321–331
[21] S.J. Gibbs, E.N. Lightfoot, T.W. Root, Protein diffusion in porous gel filtration chromatography media studied by pulsed field gradient NMR spectroscopy, J Phys Chem 96 (1992) 7458-7462.
[22] M. Camenzuli, T.A. Goodie, D.N. Bassanese, P.S. Francis, N.W. Barnett, H. Ritchie, J. LaDine, R.A. Shalliker, X.A. Conlan, The use of parallel segmented outlet flow columns for enhanced mass spectral sensitivity at high chromatographic flow rates, Rapid Commun Mass SP, 26 (2012) 043-949..
[23] R.A. Shalliker, M. Camenzuli, L. Pereira, H.J. Ritchie, Parallel segmented flow chromatography columns: Conventional analytical scale column formats presenting as a 'virtual'narrow bore column, J. Chromatogr. A 1262 (2012) 64-69.
[24] M. Camenzuli, H.J. Ritchie, J.R. Ladine, R.A. Shalliker, Enhanced separation performance using a new column technology: Parallel segmented outlet flow, J. Chromatogr. A., 1232 (2012) 47-51.
[25] R.A. Shalliker, H. Ritchie, Segmented flow and curtain flow chromatography: overcoming the wall effect and heterogeneous bed structures, J. Chromatgr. A., 1335 (2014) 122-135.
[26] G. Desmet, K. Broeckhoven, J. De Smet, S. Deridder, G.V. Baron, P. Gzil, Errors involved in the existing B-term expressions for the longitudinal diffusion in fully porous chromatographic media: Part I: Computational data in ordered pillar arrays and effective medium theory, J. Chromatogr. A, 1188 (2008) 171-188.
[27] O. Levenspiel, Chemical Reaction Engineering, 3rd ed., John Wiley & Sons, New York, NY, 1999
[28] H.S. Carslaw, J.C. Jaeger, Conduction of heat in solids, 2nd Ed., Oxford (1959), Clarendon Press.
[29] A. Klinkenberg, H.J. Krajenbrink, H.A. Lauwerier, Diffusion in a fluid moving at uniform velocity in a tube, Ind Eng Chem 45 (1953) 1202–1208.

[30] G. von Winckel, Bessel function zeros, 01/25/05 retrieved from:
http://nl.mathworks.com/matlabcentral/fileexchange/6794-bessel-function-zeros/content/besselzero.m
[31] C.N. Moore, Bull. Amer. Math. Soc., On the developments in Bessel's functions, 23 (1916) 18-27.
[32] M.E. Swartz, New frontiers in chromatography, LC GC North America, S (2005) 8.

Figure 1

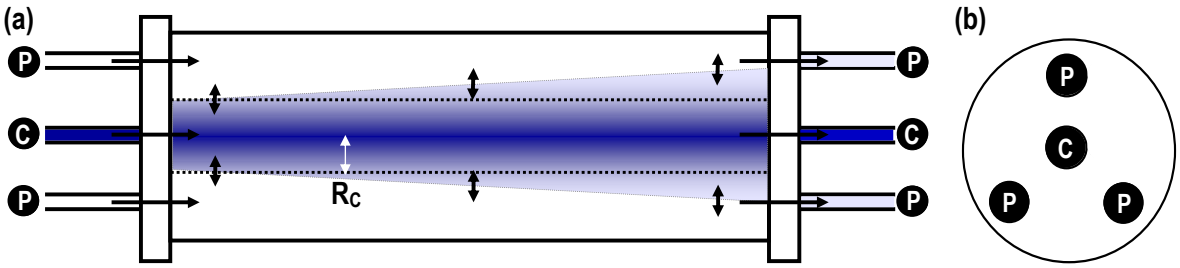

Figure 2

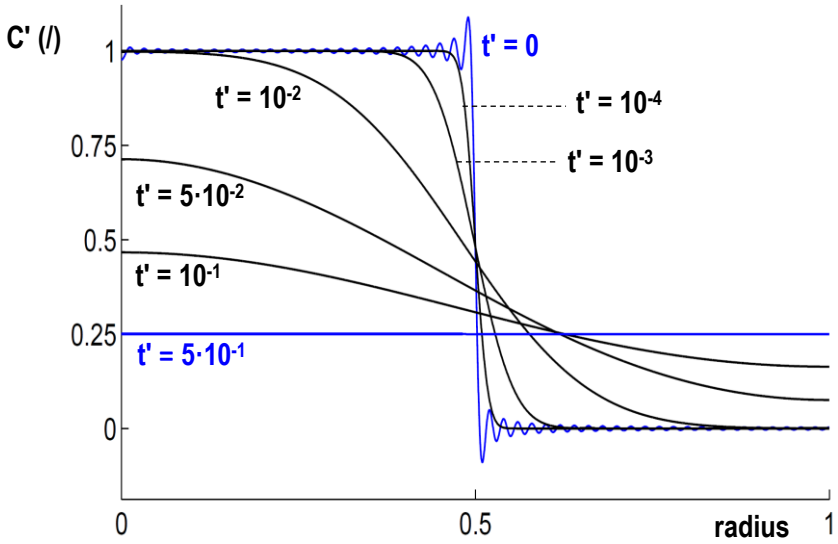
C' (l)
1
0.75
0.5
0.25
0
0
0.5
1
radius
t' = 0
t' = 10-2
t' = 10-4
t' = 10-3
t' = 5·10-2
t' = 10-1
t' = 5·10-1

Figure 3

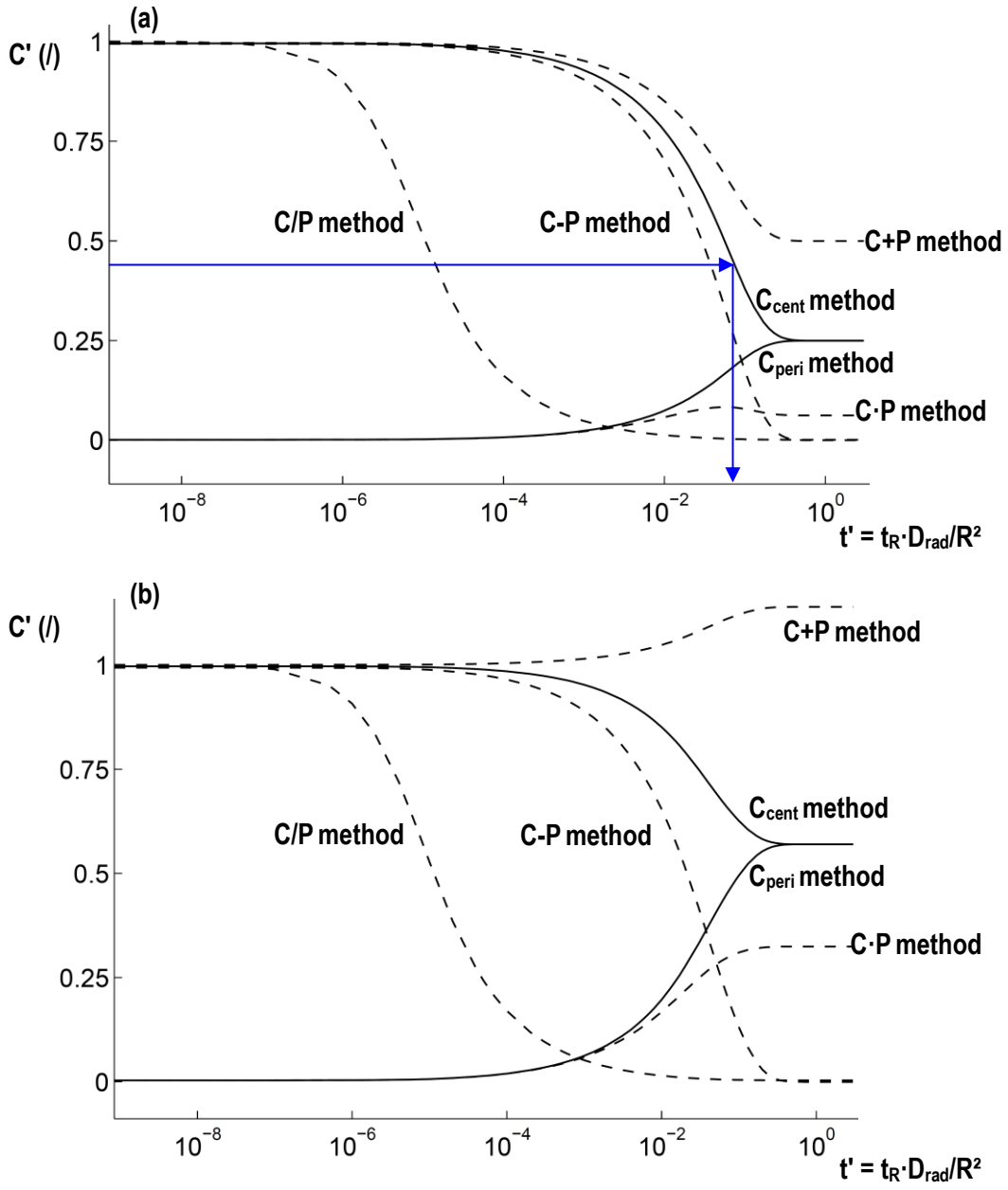
(a)
C' (/)
1
0.75
0.5
0.25
0
C/P method
C-P method
C+P method
C_cent method
C_peri method
C·P method
10^-8
10^-6
10^-4
10^-2
10^0
t' = t_R·D_rad/R²
(b)
C' (/)
1
0.75
0.5
0.25
0
C+P method
C_cent method
C/P method
C-P method
C_peri method
C·P method
10^-8
10^-6
10^-4
10^-2
10^0
t' = t_R·D_rad/R²

Figure 4

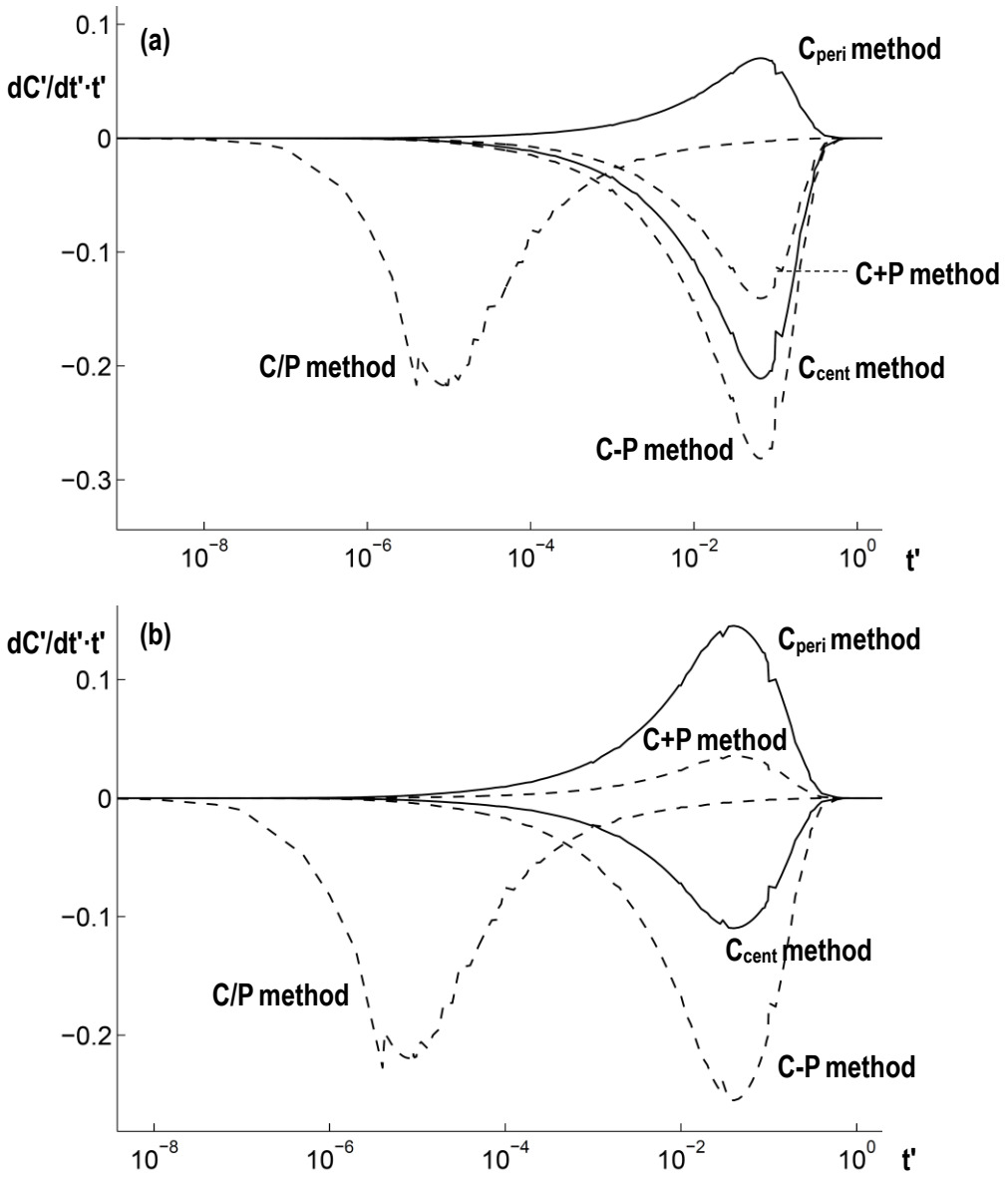
(a)
dC'/dt'·t'
0.1
0
−0.1
−0.2
−0.3
10^{-8}
10^{-6}
10^{-4}
10^{-2}
10^{0}
t'
C_{peri} method
C+P method
C/P method
C_{cent} method
C-P method
(b)
dC'/dt'·t'
0.1
0
−0.1
−0.2
10^{-8}
10^{-6}
10^{-4}
10^{-2}
10^{0}
t'
C_{peri} method
C+P method
C_{cent} method
C/P method
C-P method

Figure 5

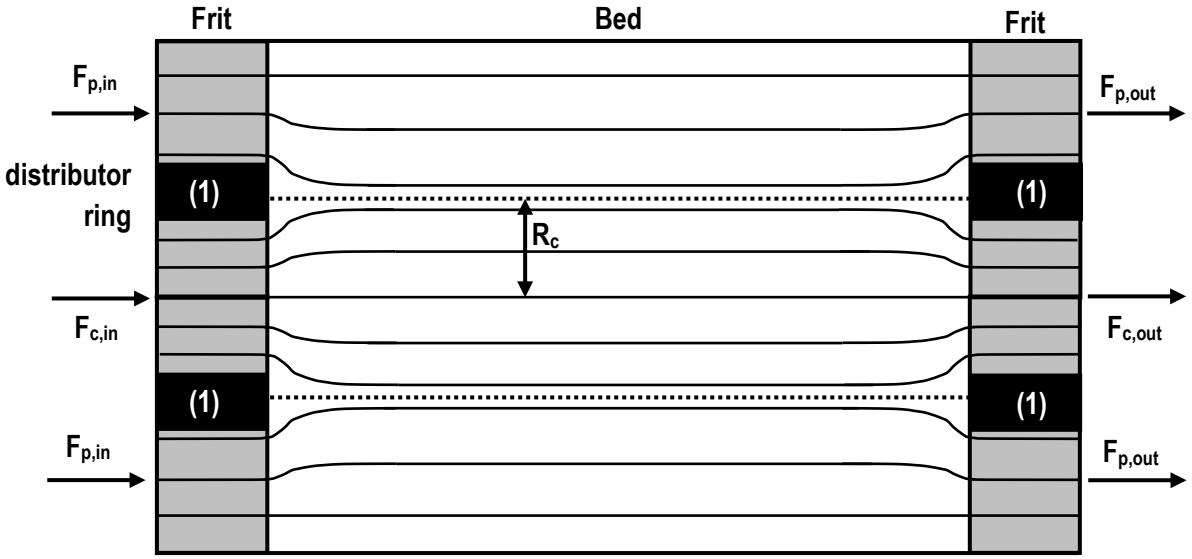
Frit
Bed
Frit
$F_{p,in}$
$F_{p,out}$
distributor ring
(1)
(1)
R_c
$F_{c,in}$
$F_{c,out}$
(1)
(1)
$F_{p,in}$
$F_{p,out}$

Figure 6

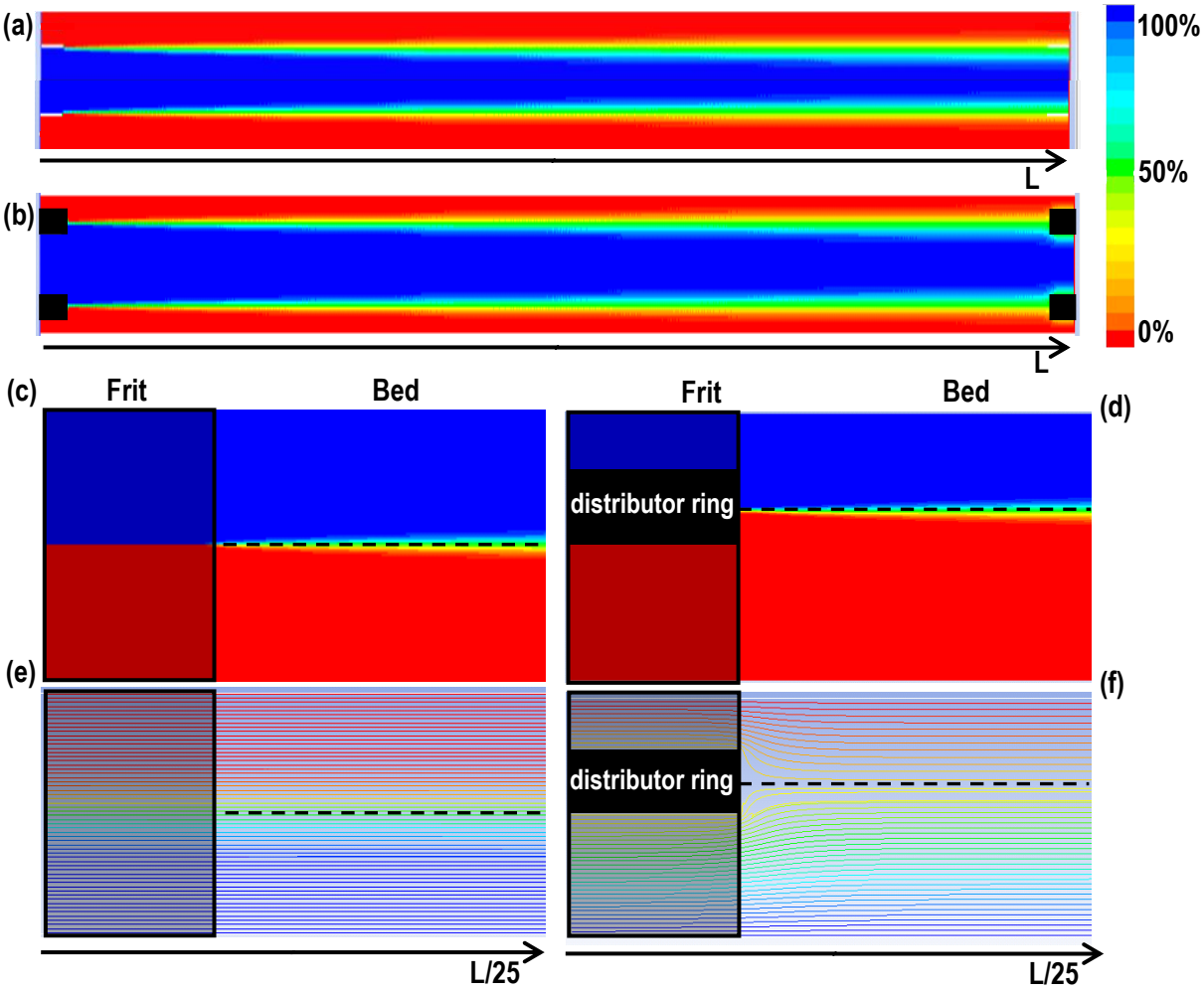
(a)
100%
50%
0%
L
(b)
L
(c)
Frit
Bed
(d)
Frit
Bed
distributor ring
(e)
(f)
distributor ring
L/25
L/25

Figure 7

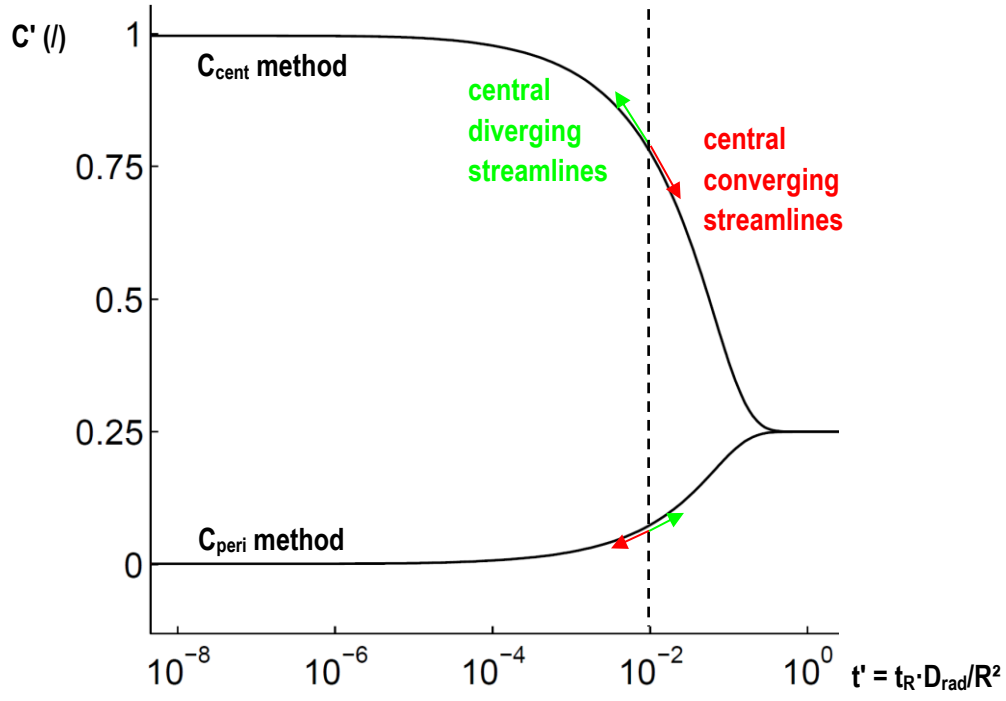
C' (/)
1
0.75
0.5
0.25
0
C_cent method
central
diverging
streamlines
central
converging
streamlines
C_peri method
10^-8
10^-6
10^-4
10^-2
10^0
t' = t_R·D_rad/R²

Figure 8

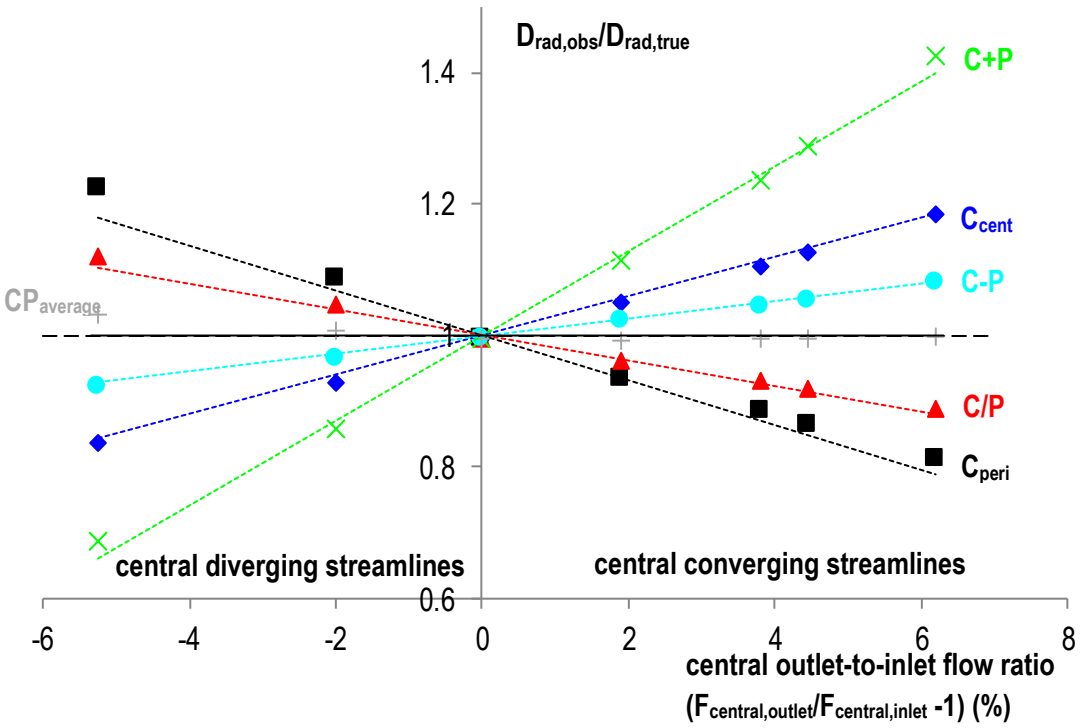
$D_{rad,obs}/D_{rad,true}$
1.4
1.2
1
0.8
0.6
$CP_{average}$
C+P
C_{cent}
C-P
C/P
C_{peri}
central diverging streamlines
central converging streamlines
-6
-4
-2
0
2
4
6
8
central outlet-to-inlet flow ratio
($F_{central,outlet}/F_{central,inlet}$ -1) (%)